

Cross-correlation of WMAP 3rd year data and the SDSS DR4 galaxy survey: new evidence for Dark Energy

A.Cabré¹, E.Gaztañaga^{1,2}, M.Manera¹, P.Fosalba¹ & F.Castander¹

¹*Institut de Ciències de l'Espai, CSIC/IEEC, Campus UAB, F. de Ciències, Torre C5 par-2, Barcelona 08193, Spain*

²*INAOE, Astrofísica, Tonantzintla, Puebla 7200, Mexico*

2 December 2024

ABSTRACT

We cross-correlate the third-year WMAP data with galaxy samples extracted from the SDSS DR4 covering 13% of the sky, increasing by a factor of 3.7 the volume sampled in previous analyses. The new measurements confirm a positive cross-correlation with higher significance (total signal-to-noise of about 4.7). The correlation as a function of angular scale is well fitted by the integrated Sachs-Wolfe (ISW) effect for LCDM flat FRW models with a cosmological constant ($w = -1$). The combined analysis of different samples gives $\Omega_\Lambda = 0.75 - 0.80$ (68% Confidence Level, CL) or $0.70 - 0.82$ (95% CL). We find that the best fit Ω_Λ decreases from 0.82 to 0.75 (95% CL) when we increase the median redshift of the galaxy sample from $z \simeq 0.3$ to $z \simeq 0.5$. The quick drop of the measured signal with z is too fast for the LCDM cosmology. The data can be better reconciled with a model with an effective dark energy equation of state $w < -1.5$. Such phantom cosmology reduces by up to $\sim 20\%$ the amplitude of the lower multipoles of the CMB temperature anisotropies with respect the $w = -1$ prediction, which also brings the models closer to the observations.

1 INTRODUCTION

Models with late time cosmic acceleration, such as the Λ -dominated CDM model, predict a slow down for the growth of linear gravitational potential at moderate redshift $z < 1$, which can be observed as temperature anisotropies in the CMB: the so-called late integrated Sachs-Wolfe (ISW) effect. The ISW effect is expected to produce an increase of power (a bump) in the amplitude of the CMB fluctuations at the largest scales, ie lower order multipoles, which are dominated by cosmic variance. This expectation, seems challenged by observations, as the first year WMAP results (WMAP1) confirmed the low amplitude of the CMB quadrupole first measured by COBE (eg Hinshaw et al. 1996a). The discrepancy between the observations and the Λ CDM model is particularly evident in the temperature angular correlation function $w_2(\theta)$, which shows an almost complete lack of signal on angular scales $\theta \gtrsim 60$ degrees. According to Spergel et al. (2003), the probability of finding such a result in a spatially-flat Λ CDM cosmology is about 1.5×10^{-3} . This was questioned in Gaztañaga et al. (2003) who found, using simulated Λ CDM WMAP maps, a much lower significance (less than 2-sigma) for $w_2(\theta)$. A low significance was also estimated by different studies (eg Efstathiou 2003, Olivera-Costa et al. 2003), although a discrepancy larger than 3-sigma still remains on both the quadrupole-octopole alignment (Tegmark, Oliera-Costa & Hamilton 2003, Olivera-Costa et al. 2003) and the WMAP

observed high value of the temperature-polarization cross-correlation on large scales (Doré, Holder & Loeb 2004).

Given the observed anomalies on the ISW predictions, it is of particular interest to check if the ISW effect can be detected observationally through an independent test, such as the cross-correlation of temperature fluctuations with local tracers of the gravitational potential (Crittenden & Turok 1996). A positive cross-correlation between WMAP1 and galaxy samples from the Sloan Digital Sky Survey (SDSS) was first found by Fosalba, Gaztañaga & Castander (2003, FGC03 from now on) and Scranton et al. (2003). FGC03 used the 1yr WMAP data (WMAP1) and the SDSS data release 1 (SDSS1). WMAP1 has also been correlated with infrared galaxies (Afshordi et al 2004), radio galaxies (Nolta et al 2004), and hard X-ray background (Boughn & Crittenden 2004; Boughn & Crittenden 2004). The significance of these cross-correlations measurements was low (about 2-3 σ , see Gaztañaga, Manera & Multamäki 2006 for a summary and jointed analysis), and many scientists are still skeptical of the reality of these findings. Here we want to check if these results can be confirmed to higher significance using the SDSS data release 4 (SDSS4) which covers 3 times the volume of SDSS1. At the same time, we will compare the signal of the 1st and 3rd year WMAP data (WMAP3) recently made public (Hinshaw et al. 2006; Spergel et al 2006). With better signal-to-noise and better understanding of foreground contamination in WMAP3, it remains to be seen whether the low significance signal of the WMAP1-

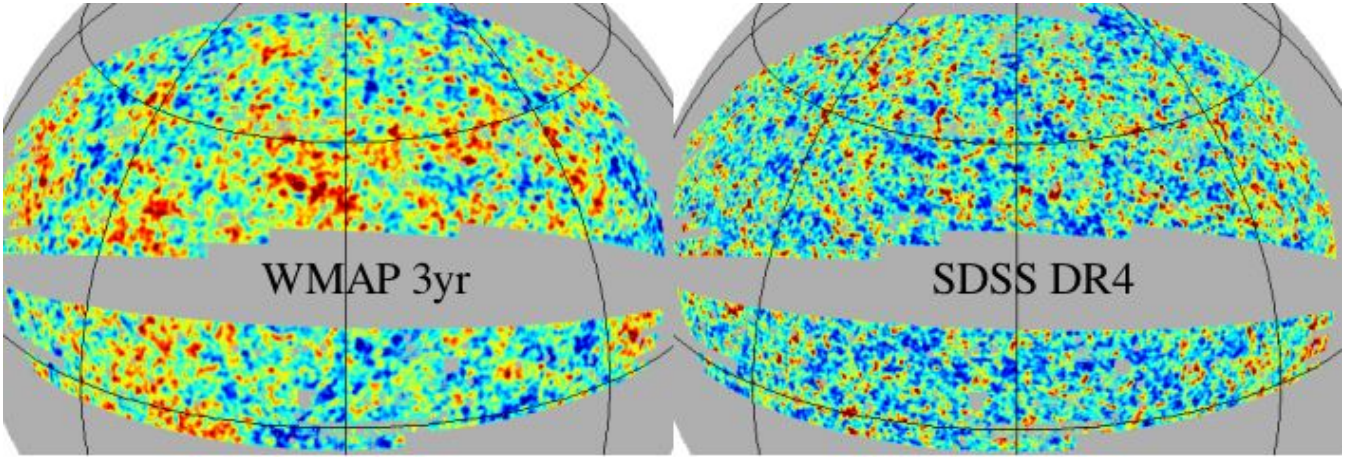


Figure 1. SDSS DR4 galaxy density (LRG) fluctuation maps (right panel) compared to WMAP (V-band 3yr) temperature map (left panel). Both maps are smoothed with a Gaussian beam of FWHM = 0.3 deg.

SDSS1 analysis can be confirmed with WMAP3-SDSS4, or if on the contrary this signal vanishes as systematic and statistical errors are reduced.

2 THE DATA

In order to trace the changing gravitational potentials we use galaxies selected from the Sloan Digital Sky Survey Data Release 4 (Adelman-McCarthy et al. 2006), SDSS4 hereafter, which covers 6670 deg² (i.e. 16% of the sky). We have selected subsamples with different redshift distributions to check the reliability of the detection and to probe the evolution of the ISW effect. All subsamples studied contain large number of galaxies, 10⁶-10⁷, depending on the subsample. We concentrate our analysis on the North Galactic Cap SDSS4 Area (~ 5500 deg²), because it contains the most contiguous area. We have selected 3 magnitude subsamples with $r = 18 - 19$, $r = 19 - 20$ and $r = 20 - 21$ and a high redshift Luminous Red Galaxy (LRG; e.g. Eisenstein et al. 2001) color selected subsample ($17 < r < 21$, $(g - r) > 0.72 * (r - i) + 1.7$, $(r - i) > (g - r)/4 + 0.36$). Because of the smaller volume, the $r = 18 - 19$ and $r = 19 - 20$ subsamples provide low signal-to-noise (S/N < 2) in the cross-correlation with WMAP, and we therefore center our analysis on the two deeper subsamples. The redshift distribution of the $r = 20 - 21$ subsample has median redshift, $z \simeq 0.3$ (e.g., Dodelson et al. 2001, Brown et al. 2003) and the LRG subsample $z \simeq 0.5$. The mask used for these data avoids pixels with observational holes, trails, bleeding, bright stars or seeing greater than 1.8.

We use the full-sky CMB maps from the third-year WMAP data (Hinshaw et al. 2006; Spergel et al. 2006) (WMAP3 from now on). In particular, we have chosen the V-band (~ 61 GHz) for our analysis since it has a lower pixel noise than the highest frequency W-band (~ 94 GHz), while it has sufficient high spatial resolution (21') to map the typical Abell cluster radius at the mean SDSS depth. We use a combined SDSS+WMAP mask that includes the Kp0 mask, which cuts 21.4% of WMAP sky pixels (Bennett

et al. 2003b), to make sure Galactic emission does not affect our analysis. WMAP and SDSS data are digitized into 7' pixels using the HEALPix tessellation ¹. Figure 1 shows how the WMAP3 and SDSS4 pixel maps look like when density and temperature fluctuations are smoothed on 0.3 deg scale.

3 CROSS-CORRELATION AND ERRORS

We define the cross-correlation function as the expectation value of density fluctuations $\delta_G = N_G / \langle N_G \rangle - 1$ and temperature anisotropies $\Delta_T = T - T_0$ (in μK) at two positions \hat{n}_1 and \hat{n}_2 in the sky: $w_{TG}(\theta) \equiv \langle \Delta_T(\hat{n}_1) \delta_G(\hat{n}_2) \rangle$, where $\theta = |\hat{n}_2 - \hat{n}_1|$, assuming that the distribution is statistically isotropic. To estimate $w_{TG}(\theta)$ from the pixel maps we use:

$$w_{TG}(\theta) = \frac{\sum_{i,j} \Delta_T(\hat{n}_i) \delta_G(\hat{n}_j) w_i w_j}{\sum_{i,j} w_i w_j}, \quad (1)$$

where the sum extends to all pairs i, j separated by $\theta \pm \Delta\theta$. The weights w_i can be used to minimize the variance when the pixel noise is not uniform, however this introduces larger cosmic variance. Here we follow the WMAP team and use uniform weights (i.e. $w_i = 1$). The resulting correlation is displayed in Fig. 2. On scales up to 10 degrees we find significant correlation above the estimated error-bars. The dotted and continuous lines correspond to WMAP1 and WMAP3 data respectively, and show little difference within the errors. This indicates that the cross-correlation is signal dominated. Compare with previous results for WMAP1-SDSS1 by FGC03

We have used different prescription for the (covariance matrix) error estimation: a) jack-knife, b) 2000 realistic simulations with the appropriate cross-correlation signal c) the-

¹ Some of the results in this paper have been derived using HEALPix (G  rski et al. 1998), <http://www.eso.org/science/healpix>

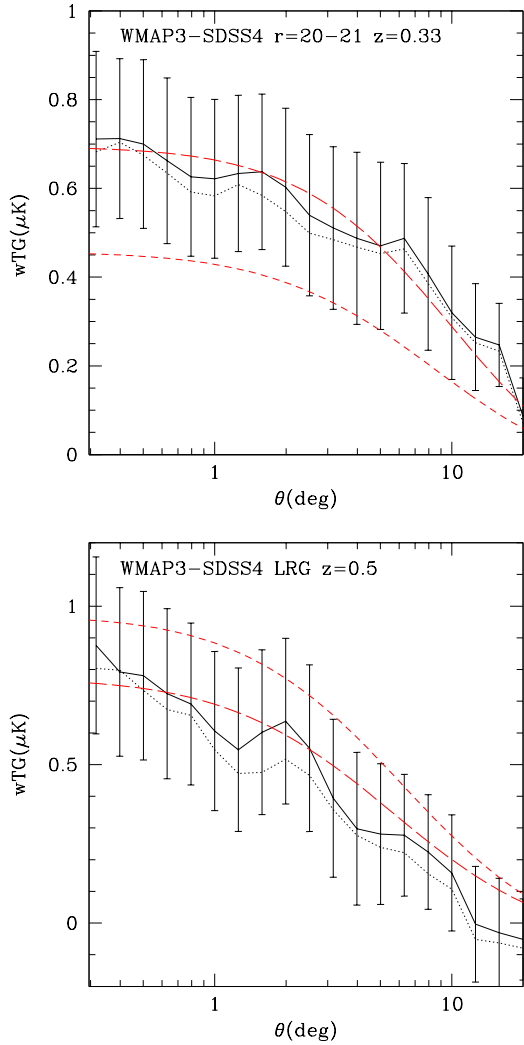


Figure 2. The continuous line with errorbars shows the WMAP3-SDSS4 angular cross-correlation as a function of scale for the $r = 20 - 21$ sample (top) and the LRG sample (bottom). The dotted line corresponds to using the 1st yr WMAP (WMAP1-SDSS4) data, which is very close to the WMAP3 results (continuous line). The short dashed lines show the Λ CDM model with $\Omega_\Lambda = 0.78$ (best overall fit) while the long-dashed lines show the best fit for each slice (ie $\Omega_\Lambda = 0.82$ and $\Omega_\Lambda = 0.75$ respectively).

oretical estimation (including cross-correlation signal) both in configuration and harmonic space. All estimates give very similar results and details will be presented elsewhere (Fosalba et al. 2006).

To compare models we use a χ^2 test:

$$\chi^2 = \sum_{i,j=1}^N \Delta_i C_{ij}^{-1} \Delta_j, \quad (2)$$

where $\Delta_i \equiv w_{TG}^E(\theta_i) - w_{TG}^M(\theta_i)$ is the difference between the "estimation" E and the model M . We perform a Singular Value Decomposition (SVD) of the covariance matrix $C_{ij} = (U_{ik})^\dagger D_{kl} V_{lj}$ where $D_{ij} = \lambda_i^2 \delta_{ij}$ is a diagonal matrix

$\theta(\text{deg})$	$wTG(20 - 21)$	$wTG(LRG)$
0.316	0.711 ± 0.198	0.876 ± 0.279
0.398	0.712 ± 0.180	0.793 ± 0.266
0.501	0.700 ± 0.190	0.781 ± 0.266
0.631	0.662 ± 0.187	0.724 ± 0.268
0.794	0.626 ± 0.179	0.691 ± 0.255
1.000	0.622 ± 0.179	0.606 ± 0.251
1.259	0.634 ± 0.176	0.547 ± 0.258
1.585	0.637 ± 0.175	0.602 ± 0.260
1.995	0.603 ± 0.178	0.637 ± 0.261
2.512	0.540 ± 0.182	0.552 ± 0.263
3.162	0.511 ± 0.183	0.394 ± 0.249
3.981	0.488 ± 0.194	0.298 ± 0.241
5.012	0.470 ± 0.188	0.281 ± 0.222
6.310	0.488 ± 0.168	0.277 ± 0.192
7.943	0.407 ± 0.172	0.224 ± 0.181
10.000	0.320 ± 0.150	0.158 ± 0.183
12.589	0.265 ± 0.121	-0.004 ± 0.182
15.849	0.247 ± 0.094	-0.031 ± 0.172
19.953	0.086 ± 0.087	-0.052 ± 0.128

Table 1. $wTG(\theta)$ for WMAP3-SDSS4.

with the singular values on the diagonal, and U and V are orthogonal matrices that span the range and nullspace of C_{ij} . We can choose the number of eigenvectors $\widehat{w}_{TG}(i)$ (or principal components) we wish to include in our χ^2 by effectively setting the corresponding inverses of the small singular values to zero. In practice, we work only with the subspace of "dominant modes" which have a significant "signal-to-noise" (S/N). The S/N of each eigenmode, labeled by i , is:

$$\left(\frac{S}{N}\right)_i = \left| \frac{\widehat{w}_{TG}(i)}{\lambda_i} \right| = \left| \frac{1}{\lambda_i} \sum_{j=1}^{N_b} U_{ji} \frac{w_{TG}(j)}{\sigma_w(j)} \right|. \quad (3)$$

As S/N depends strongly on the assumed cosmological model, we use the direct measurements of w_{TG} to estimate this quantity. The total S/N can be obtained by adding the individual modes in quadrature. When we use only the dominant eigenmodes, the total S/N estimate corresponds to a lower bound, which is not optimal, but avoids potential errors of a singular inversion. We have also checked that this approach, in configuration space, gives equivalent results to the use of spherical harmonic decomposition (see Fosalba et al. 2006).

Fig.3 shows the dominant eigenvectors in our analysis. The one with the largest S/N is the one which is practically constant as a function of angular scale: this represents the overall amplitude of w_{TG} .

3.1 Comparison with Predictions

ISW temperature anisotropies are given by (Sachs & Wolfe 1967):

$$\Delta_T^{ISW}(\hat{n}) \equiv \frac{T(\hat{n}) - T_0}{T_0} = -2 \int dz \frac{d\Phi}{dz}(\hat{n}, z) \quad (4)$$

where Φ is the Newtonian gravitational potential at redshift z . One way to detect the ISW effect is to cross-correlate tem-

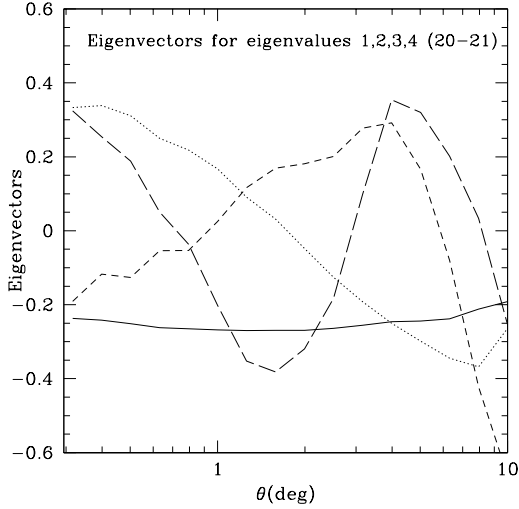


Figure 3. First four eigenvectors $\hat{w}_{TG}(i)$ (or principal components) with higher S/N in the SVD of the cross-correlation covariance matrix.

perature fluctuations with galaxy density fluctuations projected in the sky (Crittenden & Turok 1996). It is useful to expand w_{TG} in a Legendre polynomial basis. On large linear scales and small angular separations, the cross-correlation $w_{TG}^{ISW}(\theta) = \langle \Delta_T^{ISW}(\hat{n}_1) \delta_G(\hat{n}_2) \rangle$ is:

$$\begin{aligned} w_{TG}^{ISW}(\theta) &= \sum_l \frac{2l+1}{4\pi} p_l(\cos \theta) C_{GT}^{ISW}(l) \\ C_{GT}^{ISW}(l) &= \frac{4}{(2l+1)^2} \int dz W_{ISW}(z) W_G(z) \frac{H(z)}{c} P(k) \\ W_{ISW}(z) &= 3\Omega_m (H_0/c)^2 \frac{d[D(z)/a]}{dz} \\ W_G(z) &= b(z) \phi_G(z) D(z), \end{aligned} \quad (5)$$

where $k = \frac{l+1/2}{r}$, ϕ_G is the survey galaxy selection function along the line of sight z , $r(z)$ is the comoving distance. This is just a Legendre decomposition of the equations presented in Fosalba & Gaztañaga (2004), see also Afshordi (2004). The advantage of this formulation is that we can here set the monopole ($l = 0$) and dipole ($l = 1$) contribution to zero, as it is done in the WMAP maps. The contribution of the monopole and dipole to w_{TG} is significant and over predicts w_{TG} by about 10%. The power spectrum is $P(k) = A k^{n_s} T^2(k)$, where $T(k)$ is the Λ CDM transfer function, which we evaluate using the fitting formulas of Einseinstein & Hu 1998. W_{ISW} decreases as a function of increasing redshift and goes to zero both for $\Omega_m \rightarrow 0$ and for $\Omega_m \rightarrow 1$.

We make the assumption that on very large scales the galaxy distribution is a tracer of the underlying matter fluctuations, related through the linear bias factor, $\delta_G(\hat{n}, z) = b(z) \delta_m(\hat{n}, z)$. We estimate $b(z)$ from the angular galaxy-galaxy auto-correlation $w_{GG}(\theta)$ in each sample by fitting to the linear flat Λ CDM model prediction $w_{GG}(\theta)$ and marginalizing over the value of Ω_m . The models have $h = 0.71$, $T_{CMB} = 2.725$, $\Omega_B = 0.022/h^2$, $n_s = 0.938$ and

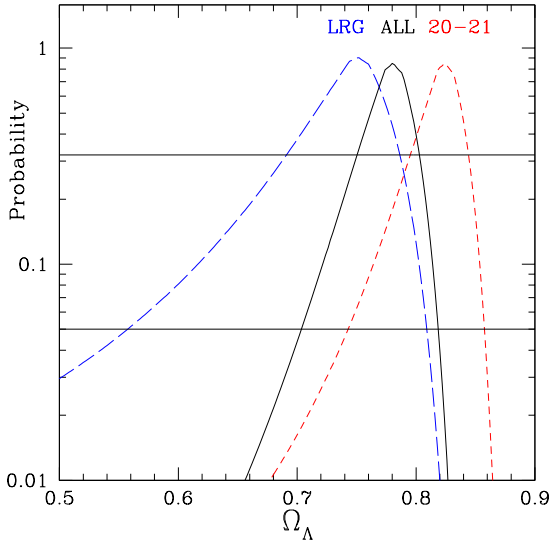


Figure 4. Probability distribution for Ω_Λ in the $r = 20 - 21$ sample (short-dashed line), the LRG sample (long-dashed line) and the combined analysis (continuous middle curve).

$\Omega_k = 0$, and are normalized to the value of σ_8 that best fits WMAP3 data (Spergel et al. 2006): $\sigma_8 = 0.75 \pm 0.03$. With this procedure we find a normalization of $b\sigma_8 \simeq 0.90 - 0.96$ and $b\sigma_8 \simeq 2.32 - 2.42$ for the $r = 20 - 21$ and LRG samples respectively. We marginalize all our results over the uncertainties in σ_8 and $b\sigma_8$. We have also tested the best fit WMAP3 data with $n_s = 1$ which gives different parameters and normalization ($\sigma_8 = 0.79 \pm 0.05$) and find very similar results.

Under the above assumptions we are left with only one free parameter, which is Ω_m or $\Omega_\Lambda = 1 - \Omega_m$. The prediction for different Ω_Λ , scaled to the appropriate bias and projected to each sample redshift, are shown as dashed lines in Fig.2. Fig.4 shows the probability distribution estimated from the $\Delta\chi^2 = \chi^2 - \chi^2_{min}$ analysis away from the minimum value χ^2_{min} . The combined best fit model has $\Omega_\Lambda \simeq 0.78^{+0.02}_{-0.03}$ and is displayed as a short dashed line in Fig.2

Fig.5 shows the joint 2D contours for dark energy models with an effective equation of state $w = p/\rho$, and a Hubble equation: $H^2/H_0^2 = \Omega(1+z)^3 + \Omega_\Lambda(1+z)^{3(1+w)}$. The Λ CDM model ($w = -1$) is disfavoured but with low significance (better than 95% when marginalized over Ω_Λ) and the best fit model prefers $w < -1.5$ and $\Omega_\Lambda > 0.8$. These constraints are similar to the ones found by Corasaniti, Giannantonio and Melchiorri (2005) and Gaztañaga, Manera & Multamäki (2006) over a compilation of cross-correlation measurements.

4 DISCUSSION

The objective of our analysis was primarily to check if we could confirm or refute with higher significance the findings of the WMAP1-SDSS1 cross-correlation by FGC03. With an increase in area of a factor of $\simeq 3.7$ in SDSS4, larger

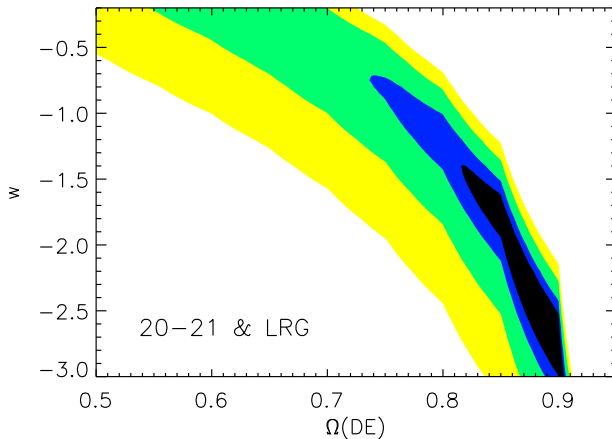


Figure 5. Two dimensional contours for Ω_Λ and w , the DE effective equation of state. The inner black contour limits the 1D marginalized 68% confidence region ($\Delta\chi^2 = 1$). The other contours correspond to: $\Delta\chi^2 = 2.3, 6.2$ and 11.8 .

signal-to-noise and better understanding of foregrounds in WMAP3, our new analysis shows that the signal is robust. This is also in line with the first findings using optical (APM) galaxies by Fosalba & Gaztañaga (2004). The cross-correlation signal in WMAP3-SDSS4 seems slightly larger for the $r = 20 - 21$ sample than in WMAP1-SDSS1 (see FGC03). The total S/N in Eq.3 of the WMAP3-SDSS4 correlation is $S/N \simeq 3.6$ for the $r = 20 - 21$ sample and $S/N \simeq 3.0$ for the LRG, which gives a combined $S/N \simeq 4.7$. This assumes that there is little correlation between the two samples which is a reasonable assumption given the difference in the comoving volume they expand. We have checked the validity of this assumption by cross-correlating both galaxy samples. We find negligible correlations on scales above 3 degrees (and less than 10% below 3 degrees).

We find (see Fig.4) that the LRG sample ($z \simeq 0.5$) prefers lower values for the cosmological constant ($\Omega_\Lambda = 0.75$) than the lower redshift galaxies ($\Omega_\Lambda = 0.82$ for $z \simeq 0.3$). This is illustrated by Fig.2, which shows how the observations lie well above (or below) the global best fit value of $\Omega_\Lambda = 0.78$ for high (or low) redshifts. This is only a 2-sigma effect but it might be a first indication for dark energy with an effective equation of state away from the Λ CDM model. The ISW effect (ie W_{ISW} in Eq.[5]) decreases more rapidly as a function of redshift for more negative values of w (see Fig.2 in Gaztañaga et al. 2006). This results in lower amplitudes for w_{TG} at larger redshifts for $w < -1$, just as we observed in our analysis. This lower amplitude results in a lower effective Ω_Λ when fitted with $w = -1$. Values of $w < -1.5$ seem to reproduce better the observed trend with redshift but the errors do not allow us to make a strong case yet (see Fig.5).

We also note that for a fix large value of Ω_Λ , a model with a more negative DE equation of state $w < -1.5$ generates 20% lower quadrupole and octopole in the CMB temperature spectrum than the corresponding $w = -1$ model.

This could also help alleviating the anomalies in the CMB anisotropies mentioned in the introduction.

In the near future, a Dark Energy Survey (DES, www.darkenergysurvey.org), with deeper galaxy samples and photometric redshift information should be able to tell us how robust are the observed deviations away from Λ CDM models.

ACKNOWLEDGMENTS

We acknowledge the support from Spanish Ministerio de Ciencia y Tecnología (MEC), project AYA2005-09413-C02-01 with EC-FEDER funding. AC and MM knowledge support from DURSI dpt of Generalitat de Catalunya and European Social Fund.

REFERENCES

Adelman-McCarthy, J. K., et al. 2006, ApJS, 162, 38
 Afshordi, N., Loh, Y., Strauss, M.A., 2004, Phys. Rev D 69, 083524
 Afshordi,N., 2004 astro-ph/0401166.
 Bennett, C. L., et al. 2003b, ApJ.Suppl., 148, 97
 Boughn, S. P. & Crittenden, R. G. 2004, Nature, 427, 45
 Boughn, S.P. & Crittenden, R. G., 2004, ApJ 612, 647-651
 Brown, M. L., et al. 2003, MNRAS, 341, 100
 Corasaniti, P.S., Giannantonio, T., Melchiorri, A. 2005, Phys. Rev D 72, 023514
 Crittenden, R. G., Turok, N., 1996, PRL, 76, 575
 Dodelson, S. et al. 2002, ApJ, 572, 140
 Efstathiou, 2003, MNRAS, 346, L26
 Eisenstein, D.J., et al, 2001, AJ, 122, 2267
 Fosalba, P., & Gaztañaga, E., 2004, MNRAS, 350, L37
 Fosalba P., Gaztañaga E., Castander F., 2003, ApJ, 597, L89
 Fosalba, P. et al. 2006, in preparation
 Gaztañaga E., Wagg, J., Multamäki, T., Montaña, A., Hughes, D.H., 2003, MNRAS, 346, 47
 Gaztañaga E., Manera, M. & Multamäki, T., 2006, MNRAS, 365, 171
 Górski, K. M., Hivon, E., & Wandelt, B. D. 1999, in Proc. MPA-ESO Conf., Evolution of Large-Scale Structure: From Recombination to Garching, p.37, Ed. A.J.Banday, R.K.Seth, & L.A.N. da Costa (Enschede: PrintPartners Ipskamp)
 Hinshaw, G. F. et al. 2003, ApJ.Suppl., 148, 63
 Hinshaw et al. , 2006, astro-ph/0603451
 Nolta M.R., et al., 2004, ApJ 608, 10
 Oliveira-Costa, A., Tegmark, M., Zaldarriaga, M., Hamilton, A., 2004, PRD, 69, 063516
 Sachs, R. K. & Wolfe, A. M. 1967, ApJ, 147, 73
 Scranton et al. 2003, astro-ph/0307335.
 Spergel et al. 2006, astro-ph/0603449
 Tegmark, M., Oliveira-Costa, A., Hamilton, A., 2003, PRD, 68, 123523